Shaping substrate selectivity in a broad spectrum metallo-β-lactamase

Lisandro J. González[1,2], Cintia Stival V.[1], Juan L. Puzzolo[3], Diego M. Moreno[3,4], Alejandro J. Vila[1,2,#].

[1]Instituto de Biología Molecular y Celular de Rosario (IBR, CONICET-UNR), Ocampo y Esmeralda, predio CCT, 2000 Rosario, Argentina.

[2]Área Biofísica, Facultad de Ciencias Bioquímicas y Farmacéuticas, Universidad Nacional de Rosario, Suipacha 531, S2002LRK Rosario, Santa Fe, Argentina.

[3]Instituto de Química Rosario (IQUIR, CONICET-UNR), Suipacha 570, S2002LRK Rosario, Santa Fe, Argentina.

[4]Área Química General e Inorgánica, Facultad de Ciencias Bioquímicas y Farmacéuticas, Universidad Nacional de Rosario, Suipacha 531, S2002LRK Rosario, Santa Fe, Argentina.

Running Title: Shaping the substrate profile of MBLs

Address correspondence to Alejandro J. Vila, vila@ibr-conicet.gov.ar

ABSTRACT

Metallo-β-lactamases (MBLs) are the major group of carbapenemases produced by bacterial pathogens. The design of MBL inhibitors has been limited, among other issues, by the incomplete knowledge about how these enzymes modulate substrate recognition. While most MBLs are broad-spectrum enzymes, B2 MBLs are exclusive carbapenemases. This narrower substrate profile has been attributed to a sequence insertion present in B2 enzymes that limits the accessibility to the active site. In this work, we evaluate the role of sequence insertions naturally occurring in the B2 enzyme Sfh-I and in the broad-spectrum B1 enzyme SPM-1. We engineered a chimeric protein in which the sequence insertion of SPM-1 was replaced by the one present in Sfh-I. The chimeric variant is a selective cephalosporinase, revealing that the substrate profile of MBLs can be further tuned depending on the protein context. These results also show that the stable scaffold of MBLs allows a modular engineering much richer than the one observed in nature.

INTRODUCTION

The worldwide spread of resistance to antibiotics has raised a global concern, particularly regarding carbapenem-resistant Enterobacteriaceae. The largest group of carbapenemases is comprised by metallo-β-lactamases (MBLs) (1), which are Zn(II)-dependent β-lactamases able to hydrolyze most β-lactam drugs (2, 3). MBL genes, which are common in environmental bacteria, have disseminated into MDR Gram-negative pathogens helped by mobile genetic elements. Outbreaks of multirresistant Enterobacteriaceae, *Pseudomonas aeruginosa* or *Acinetobacter baumanii* producing NDMs, VIMs, IMPs or SPM-1 MBLs are ubiquitous worldwide (4). Most worrisome, no clinical inhibitors against these enzymes are available (3).

MBLs share a general protein fold and an active site where one or two Zn(II) ions are required for substrate binding and catalysis (2, 5). Within this common fold, the surroundings of the active site are highly variable and impact on the substrate and inhibition profiles (6), and in the host adaptability of these enzymes (7). These variable regions dictate the clinical evolution of MBLs as they include most of the mutational hotspots (8–11). Despite their relevance, the role of individual residues or loop-structures around the active site is incompletely understood, limiting our knowledge on how MBLs modulate their substrate profile, and ultimately hindering the design of a common inhibitor (6, 12). Understanding the molecular features that shape the substrate profile of MBLs appears also as a challenge to comprehend the evolution of these enzymes (7).

The structural diversity of MBLs has led to a classification into three subclasses: B1, B2 and B3, each one with a unique arrangement of conserved metal ligands, loops and a set of second-shell residues around the active site, that define the substrate specificity (2, 6). B1 MBLs (the most clinically relevant MBLs) contain a solvent-accessible active site located on a shallow groove between two flexible loops (L3 and L10) and bind two Zn(II) ions (13). Their active sites

can accommodate different types of β-lactam antibiotics (penicillins, carbapenems and cephalosporins), thus being broad-spectrum enzymes. In a similar way, B3 bimetallic active sites are solvent-accessible and are broad-spectrum, despite bearing a different loop architecture (2, 6). B2 subclass MBLs, instead, are exclusive carbapenemases and only bind one Zn(II) in their active form. These enzymes harbor a truncated L3 loop and a sequence insertion in the active site (between helix α3 and β-strand β7) that introduces a "kink" generating a hydrophobic wall on the active site surface. This architecture is thought to determine the narrow substrate profile of B2 enzymes (2, 13).

P. aeruginosa SPM-1 is unique among B1 enzymes in that it possesses a loop arrangement reminiscent of B2 enzymes, i.e., a shortened L3 loop and a sequence insertion between helix α3 and β-strand β7 (14). Indeed, SPM-1 has been considered as a hybrid enzyme between B1 and B2 subclasses, despite its broad substrate spectrum and metal ligands that are shared with B1 enzymes (15). However, the sequence insertion of SPM-1 differs in length and residue identity compared to B2 enzymes (24 residues in SPM-1 vs. 17 in B2 enzymes), suggesting different evolutionary origins (14). Here we used SPM-1 as a template for protein engineering in which we grafted the sequence insertion from the typical B2 enzyme Sfh-I aimed to restrict the substrate spectrum. The resulting chimeric protein (SPM-1/Sfh-I) showed indeed a narrower substrate spectrum, revealing that sequence insertion in this region affects substrate recognition in MBLs. It also reveals alternative evolutionary pathways still unexplored in nature that may benefit from the stable scaffold of MBLs to accumulate insertions, deletions and mutations giving rise to novel resistance phenotypes.

RESULTS AND DISCUSSION

Design of a chimeric protein

The chimeric SPM-1/Sfh-I protein was designed based on a structural alignment of SPM-1 and Sfh-I (PDB codes 2FHX and 3SD9, respectively) (14, 16) (Figure 1A). A segment of 31 residues, containing the native 24 aminoacids insertion, was removed from SPM-1 and replaced by the corresponding sequence from Sfh-I, substituting the entire region in which the three-dimensional arrangements of both enzymes differ. Point mutations D226F and Y223N, in L10 loop, and L119T, in L7 loop, were incorporated in SPM-1 to mimic the native interactions of the sequence insertion in Sfh-I (Figure 1B, 1C).

Resistance profile and stability of the SPM-1/Sfh-I chimera in *P. aeruginosa* and *E. coli*

We examined the ability of the mutant gene to express a stable and active protein in two different model hosts of MBL producers, *P. aeruginosa* (the natural host of SPM-1) and *Escherichia coli*. For this purpose, we used a *P. aeruginosa* PAO1 strain to produce both wild type SPM-1 and the chimeric SPM-1/Sfh-I variant. Proteins were produced fused to a C-terminal strep-tag sequence for immunoblotting detection, which does not affect the resistance profile of MBLs (17), and with the native peptide leader of SPM-1 for periplasmic localization. We measured minimal inhibitory concentration (MIC) values of different β-lactam antibiotics towards strains expressing these proteins. The SPM-1/Sfh-I chimera, unlike wild type SPM-1, was not able to confer resistance against β-lactam antibiotics in *P. aeruginosa*. MIC values of imipenem, piperacillin and ceftazidime were comparable to those of the control strain containing an empty vector. Similar results were obtained in *Escherichia coli*, revealing that inability of the chimera to confer resistance is not host-specific.

We then evaluated the stability *in vivo* of SPM-1/Sfh-I compared to wild type SPM-1 in different cell compartments. Periplasmic and spheroplast fractions of *P. aeruginosa* PAO1 and *E. coli* DH5α expressing wild type or the chimeric protein were analyzed by Western-blot using anti

Strep-tag antibodies. As shown in Figure 2, both wild-type SPM-1 and the chimera were produced to similar levels in cells, but SPM-1/Sfh-I did not accumulate in the periplasmic fraction of these bacteria, the site of action of MBLs. These results indicate that the inability to confer resistance is due to the lack of accumulation of the chimeric protein in the periplasm, likely due to stability issues that are not host-dependent.

Biochemical characterization of SPM-1 and SPM-1/Sfh-I

We then characterized biochemically the chimeric protein, to assess its activity and stability *in vitro*. Over-expression of the chimera resulted in formation of inclusion bodies indicating that the insertion introduced in the chimeric protein is destabilizing. Similar results were obtained were obtained when trying to optimize induction conditions. Thus, we attempted recovering the protein from inclusion bodies in denaturing conditions, followed by refolding in the presence of Zn(II) by flash dilution (see Material and Methods for details). The same protocol was used with wild type SPM-1 to obtain comparable results. The procedure was successful, allowing to obtain up to 5 mg per liter of culture of folded and active protein, evaluated by nitrocefin hydrolysis.

Circular dichroism (CD) in the far UV revealed the presence of secondary structure in both purified proteins (Fig. 3A). The metal content of both SPM-1/Sfh-I and wild type SPM-1 was variable among different purifications, ranging from 0.6 to 2 Zn(II) equivalents per protein, yielding an average of 1.4 Zn(II) equivalents per protein. Since B1 MBLs are prone to oxidation of the Cys221 ligand (14, 18) we measured the level of oxidation in the SPM-1/SfhI by reaction of the denatured chimera with Ellman's reagent DTNB. This revealed that 30 % ± 5 of Cys221 is oxidized showing that failure to bind two Zn(II) equivalents stems from oxidation of this residue and not from a hybrid behavior between B1 and B2 enzymes. Altogether these results indicate that SPM-1/Sfh-I has the potential to bind two Zn(II) ions, as expected for the ligand set of a B1

lactamase. The irreversible thermal denaturation of SPM-1/Sfh-I vs. the wild type protein was determined by thermal shift assays. SPM-1 displayed a very high thermal stability (T_m = 72 °C), while the melting temperature for the chimeric protein was 51 °C. Despite this value is higher than the normal growth temperature of bacterial cells, it reveals a large destabilization in the chimera, which accounts for its scarce accumulation in the bacterial periplasm. This ultimately leads to the lack of resistance observed.

***In vitro* β-lactamase activity**

The β-Lactamase activity of purified SPM-1/Sfh-I and wild type SPM-1 was determined against a wide range of β-lactam antibiotics (Table 2 and Supplementary Fig. 1). Surprisingly, in SPM-1/Sfh-I we observed substrate inhibition with cephalosporins at substrate concentrations above 100 μM, suggesting the formation of dead-end enzyme-substrate complexes (Supplementary Fig. 1). Catalytic efficiencies estimated from linear regression of the curves at [S]→0, however, revealed similar values to those measured for wild type SPM-1. In contrast, the chimeric protein displayed a large drop in the catalytic efficiencies (k_{cat}/K_M) against imipenem and penicillins (ranging between 2-3 orders of magnitude) compared to the wild type enzyme. This effect is due to a reduction in k_{cat} values for both types of substrates, and an increase in K_M only for penicillins. This suggests that the insertion of the Sfh-I sequence does not disturb binding of some substrates to the active site (as observed for B2 enzymes (19–22)), but that instead, affects their hydrolysis. Overall, SPM-1/Sfh-1 resembles B2 lactamases in that both are narrow spectrum enzymes, but while the latter are exclusive carbapenemases, the hybrid SPM-1/Sfh-I shows a clear preference for cephalosporins. Finally, the similarity in catalytic efficiencies for cephalosporins in SPM-1/Sfh-I compared to SPM-1 suggests that neither binding nor hydrolysis of these substrates involve the α3 region of MBLs.

Molecular dynamics simulations

The reduced stability of the SPM-1/Sfh-I chimera, together with the low yields of purified enzyme, limited the possibility of obtaining crystals and prevented us from using X-ray crystallography. We therefore decided to build a chimeric protein *in-silico* by homology modeling based on the reported structures of wild type SPM-1 and Sfh-I. This model was then subjected to 100 ns of Molecular Dynamics (MD) simulations using the AMBER14 package (23) at 300 K in the NVT ensemble, to observe the time evolution of its conformation. Parallel runs on wild type SPM-1 and Sfh-I were performed to specifically assess the role of the sequence insertion in the dynamics in different scaffolds. Previous work showed that the native sequence insertion of SPM-1 can adopt two conformations in equilibrium (24): one "open" (SPM-1^{open}) in which residues arrange as an extension of the α3 helix and an additional α4 helix, both exposed and oriented towards the solvent (14), and one "closed" similar to B2 enzymes (SPM-1^{closed}) (Figure 4) (24, 25). The crystal structures of both forms were used as starting geometries for separate MD runs, both for the wild type SPM-1 and the chimeric protein. Figure 4A shows representative snapshots of the MD simulations of the enzymes subject of this study. All proteins maintained their general conformation during the simulations, as seen in the temporal evolution of root means square deviation (Supplementary Figure 2A).

In order to monitor the conformation of the sequence insertion during the simulations, we analyzed the temporal evolution of the distance between the Zn(II) ions and the tip of the insertion (Supplementary Figure 2B). When simulations were started from the SPM-1^{open} structure, the sequence insertion remained in the open conformation. Likewise, simulations starting either from SPM-1^{closed} or Sfh-I showed a closed conformation invariable over time. On the contrary, in the case of SPM-1/Sfh-I chimera, the sequence insertion fluctuated between an

180 open (SPM-1/Sfh-I^{open}) and a closed (SPM-1/Sfh-I^{closed}) conformation, similar to SPM-1^{open} and
181 SPM-1^{closed} (or Sfh-I), respectively. This was evidenced as a periodic variation in the distance
182 between Zn(II) ions and the tip of the insertion. These results show that the sequence insertion in
183 the chimera gained dynamics. MD simulations allowed us to simulate different conformations to
184 later study the accessibility of the substrate by Brownian Dynamics simulation (BD) simulations.
185 BD simulations are a powerful tool for studying the motion of molecules in solution and
186 have been widely applied to study of the encounter of an enzyme and its ligand (26). In an
187 attempt to account for the impact of the insertion in the restricted activity profile of the chimera,
188 we calculated the relative probability of association of a substrate (benzylpenicillin) by BD
189 simulations, following the Zn2…N (β-lactam ring) distance as reaction criteria. We analyzed
190 2,000,000 BD trajectories to estimate the association probability. Both SPM-1^{close} and SPM-
191 1/Sfh-I^{close} show an almost null association probability. Instead, both open forms are able to bind
192 benzylpenicillin, but the association probability for SPM-1^{open} is 4-fold larger compared to that
193 of SPM-1/Sfh-I^{open} (Figure 4B). Given that BD simulations consider two features, the position
194 and the electrostatic potential of the insertion, the lower probability of association observed in
195 SPM-1/Sfh-I^{open} may be due to the different nature of the residues present in the insertion. This
196 result indicates that the insertion excludes the substrates to be hydrolyzed, in agreement with the
197 reduced catalytic efficiency observed for penicillins as substrates of SPM-1/SfhI. Due to the
198 dynamic nature of this insertion, the chimeric protein is able to hydrolyze substrates when this
199 enzyme explores the open form conformation.
200
201 **DISCUSSION**
202 The continuous molecular evolution of MBLs that might render them more stable or
203 efficient for β-lactame-hydrolysis remains a constant challenge. Because MBLs hydrolyze the

most clinical important antibiotics, understanding the determinants of their substrate profile is a major concern. It has been suggested that different protein loops, that are not necessarily part of the active site, might play a role in substrate binding, such as the mobile flap of the B1 enzymes (27). In this work, we studied the role of the sequence insertion between helix α3 and β-strand β7 on the substrate selectivity of MBLs. To this end, we constructed a chimeric protein based on a B1 scaffold (SPM-1), substituting its natural insertion sequence on the active site by that of a typical B2 enzyme (SfhI). We were able to express, purify, and characterize this construct. Despite that the change on SPM-1 represented as much as a 12.3 % modification of its primary structure, the enzyme tolerated the insertion, eliciting an active lactamase. This result confirms the proposed structural similarity between SPM-1 and B2 MBLs. The chimera retained the Zn(II) stoichiometry of B1 enzymes, showing that the insertion did not affect metal binding.

It has been suggested that the sequence insertion might constraint the B2 MBLs substrate profile to render them exclusive carbapenemases. On the other hand, a role for the natural sequence insertion in SPM-1 has not been assigned, yet it could represent a hotspot for mutations that might change substrate-profile and catalytic parameters in a context-dependent way.

The results obtained with SPM-1/Sfh-I indicate that the replacement of the native SPM-1 sequence by that of a typical B2 enzyme, significantly affected ligand binding and turnover numbers by changing the substrate profile of the enzyme. The insertion sequence excluded certain substrates from the active site in a context-dependent way; unlike B2 enzymes (exclusive carbapenemases), in the surroundings of SPM-1 this segment favors the hydrolysis of cephalosporins over penicillins and carbapenems. Compared to wild type SPM-1, the hybrid MBL revealed a sharp decrease on k_{cat}/K_M values of 48 times for penicillin G and 34 times for piperacillin. These reductions in the catalytic efficiency values were associated to a major increase in K_M and, less significantly to an increase in the turnover number. Thus, the presence

of the typical B2 sequence insertion restricted the access of penicillins to the active site, even within the context of a B1-subclass enzyme.

In the case of imipenem, the loop change did not affect the antibiotic binding as reflected in K_M values, but still presented a 17-fold decrease on k_{cat}/K_M attributable to an increase in the turnover. These results suggest that imipenem binding could be independent of residues in the native sequence insertion of SPM-1. Alternatively, K_M values could indicate that the B2 sequence insertion in the chimera might be locking imipenem in the active site after first contacts, but not penicillins substrates. If this was the case, then B2 sequence insertion in their native context might be playing a role at securing carbapenems but not other substrates to the catalytic site. However, in the scaffold of SPM-1 the correct position of imipenem for nucleophilic attack may not be achieved, thus yielding high turnover values.

In clear contrast, cephalosporins kinetic parameters were barely affected by the presence or amino acid composition of the sequence insertion. The drop in k_{cat}/K_M values for cefotaxime increased 3-fold while it remained almost unaltered for ceftazidime. In the cases of cefuroxime and cephaloridine there was a minor drop in k_{cat}/K_M values of 3 and 5-fold, respectively.

Analysis of the catalytic parameters for cefotaxime show that there was a 5-fold increase in its K_M, while its turnover number was mostly affected by the loop modifications in SPM-1 resulting in a 13-fold increase. Thus, contrasting what was proposed for imipenem, the sequence insertion of ShfI in the context of SPM-1 might help orienting the substrate for proper hydrolysis within the active site. All the changes observed in the kinetic parameters can be attributed to the B2-insertion and not to removal of the SPM-1 stretch, since previous studies have shown that elimination of the 24-aminoacid insertion in SPM-1 did not affect significantly the enzyme activity (14).

Despite the fact that the hybrid MBL showed *in vitro* activity against cephalosporins, it did not confer resistance *in vivo*. MICs reflect not only catalytic efficiencies, but also expression levels, folding behavior, and accessibility of the enzymes to the substrates within the bacterial periplasm. Considering that bacterial cultures were grown below the melting temperature for SPM-1/Sfh-I, one could argue that under these conditions the protein should be properly folded. However, if we consider that the unfolding transition begins at approximately 37 °C, and that *in vivo* there are molecular crowding effects accelerating protein aggregation, the results obtained would account for the loss of solubility in the periplasm. In fact, a role in protein stability has been recently assigned to the α3 insertion of CphA B2 enzyme (28), further supporting this hypothesis.

The suboptimal context of the B2 insertion in the chimera unmasks different mechanisms of exclusion for each type of β-lactam antibiotics. In this way, sequence insertions in α3 may act as substrate-regulatory modules able to favor or exclude specific antibiotics in a context-dependent way. Incorporation of these modules may be an evolutionary strategy for drastic modification of substrate profiles in MBLs, followed by mutations in second-shell residues for further fine-tuning. Overall, the results reveal that there are alternative evolutionary pathways still unexplored in nature that may benefit from the stable scaffold of MBLs to accumulate insertions, deletions and mutations giving rise to novel activities or resistance phenotypes.

MATERIALS AND METHODS

Bacterial Strains and Reagents

E. coli DH5α was used for construction of plasmid pMBLe-$bla_{SPM\text{-}1/Sfh\text{-}I}$. *P. aeruginosa* PAO1 and *E. coli* DH5α were used for expression of the pMBLe-$bla_{SPM\text{-}1/Sfh\text{-}I}$ and pMBLe-$bla_{SPM\text{-}1}$ constructs in resistance and cellular fractionation studies. *E. coli* BL21 (DE3) was used

for overexpression of recombinant proteins. Unless otherwise noted, all strains were grown aerobically at 37 °C in lysogeny broth (LB) medium supplemented with gentamicin 20 μg/mL or kanamycin 50 μg/ml when necessary. Chemical reagents were purchased from Sigma-Aldrich, molecular biology enzymes from Promega, and primers from Invitrogen.

Plasmid Vectors

The nucleotidic sequence of $bla_{SPM-1/Sfh-I}$ was synthesized by Genscript (USA) and PCR-amplified with primers SPM-1*Nde*I-Fw (5′-GTACGTCATATGAATTCACCTAAATCGAGAGC-3′) and SPM-1St*Hind*III-Rv (5′-GTACGTAAGCTTCTACTTTTCGAATTGTGGGTGAGACCACAGTCTCATTTCGCCAAC-3′) for subcloning into pMBLe-bla_{SPM-1} plasmid (7) through *Nde*I and *Hind*III sites. The resulting construct, pMBLe-$bla_{SPM-1/Sfh-I}$, allows expression of SPM-1/Sfh-I with the native peptide leader of SPM-1, and fused to a Strep-Tag II sequence at the C-terminus (for comparative protein detection and quantification with respect to SPM-1). For protein overexpression, the regions coding for mature SPM-1 and SPM-1/Sfh-I were PCR-amplified from pMBLe plasmids with primers SPM-1*Nde*IFw (5′-AGTCAGTCCATATGTCGGATCATGTCGACTTGCC-3′) and SPM-1*Xho*I-Rv (5′-AGTCAGTCCTCGAGGGTTGGGGATGTGAGACTAC-3′), and subcloned into plasmid pET-28a through *Nde*I and *Xho*I sites(7). The resulting plasmids allow production of mature SPM-1 and SPM-1/Sfh-I proteins with an N-terminal thrombin-cleavable his-tag. All PCRs were carried out using Platinum Pfx DNA Polymerase (Invitrogen) with the following thermal cycle: 3 min at 95 °C, 30 cycles of 15 s at 95 °C, 30 s at 55 °C and 1 min at 68 °C, and 10 min at 68 °C. Plasmids were introduced into *E. coli* strains or *P. aeruginosa* PAO1 as previously described (29). All constructs were verified by DNA sequencing (University of Maine).

299

300 **Cellular Localization and Resistance Determination**

301 Extraction of periplasmic proteins was performed as previously described (30). Briefly,
302 2–3 mL of mid-log *P. aeruginosa* PAO1 (or *E. coli* DH5α) pMBLe-*bla* cultures were induced
303 with 20 µM IPTG for 2 hours, were pelleted and cells washed once with 20 mM Tris pH 8, 150
304 mM NaCl. Cells were resuspended in 20 mM Tris pH 8, 0.1 mM EDTA, 20% w/v sucrose, 1
305 mg/mL lysozyme (from chicken egg white, Sigma-Aldrich, protein ≥90%), 0.5 mM PMSF
306 (resuspension volume was normalized according to the formula V = 100 µL × OD600 × Vc,
307 where Vc is the starting volume of culture sample), incubated with gentle agitation at 4 °C for 30
308 min and finally harvested, obtaining the periplasmic extract in the supernatant. The pellet, which
309 consists of spheroplasts, was washed in 20 mM Tris pH 8, 0.1 mM EDTA, 20% w/v sucrose and
310 resuspended in the same volume of this buffer. MBL protein levels were determined by SDS-
311 PAGE followed by western blot with Strep-Tag II monoclonal antibodies (at 1:1,000 dilution
312 from 200 µg/mL solution) (Novagen, 71590-3) and immunoglobulin G-alkaline phosphatase
313 conjugates (at 1:3,000 dilution) (Biorad, 170-6520) in PVDF membranes (GE). Western blots
314 with antibodies detecting periplasmic maltose-binding protein (Rockland Immunochemicals,
315 200-401-385) and cytoplasmic GroEL (provided by A. Viale, IBR/CONICET-UNR) were
316 performed as loading controls for periplasmic extracts and spheroplasts, respectively.

317 β-Lactam MIC determinations were performed in LB medium supplemented with 20 µM
318 IPTG using the agar macrodilution method, according to CLSI guidelines (31).

319

320 **Purification of Wild Type SPM-1 and Chimeric SPM-1/Sfh-I Proteins**

321 An overnight culture (40 mL) of the *E. coli* BL21 (DE3) pET-28a-bla was diluted in 4
322 liters of fresh LB-kanamycin and grown with shaking at 37°C until $OD_{600\ nm}$ of 0.8. Protein

expression was induced by addition of IPTG at a final concentration of 1 mM for 4 hours at 37 °C. Bacterial cells were harvested and lysed by sonication in 30 ml of denaturating buffer containing 100 mM Tris pH 8, 100 mM phosphate, 8 M urea, 2 mM β-mercaptoethanol at 4°C. Cell debris was removed by centrifugation (20,000 rpm for 1 hour at 4°C) and proteins purified by Ni-NTA affinity cromatography (GE Healthcare) in denaturing buffer at pH 8, for loading and washing, and denaturing buffer at pH 4.5 for elution. His-tagged proteins were refolded by flash dilution in 1 L of refolding buffer (50 mM HEPES pH 7.5, 200 mM NaCl, 2 mM β-mercaptoethanol, 5 mM imidazole) supplemented with 5 mM imidazole and 100 µM $ZnSO_4$, at 4 °C under vigorous agitation. Refolded proteins were concentrated by Ni-NTA affinity chromatography and eluted with refolding buffer containing 500 mM imidazole. His tags were cleaved by treatment with 1 mg of thrombin every 30 mg of fusion protein during 16 hours at 4 °C, and eliminated through Ni-NTA chromatography in refolding buffer supplemented with 5 mM imidazole. Purified SPM-1 and SPM-1/Sfh-I were concentrated using 10 kDa MW cutoff Centricon devices (Millipore) and dialyzed against 50 mM HEPES pH 7.5, 200 mM NaCl for further experiments. Protein concentrations were determined from absorbance at 280 nm using a molar absorption coefficient ($\varepsilon_{280\ nm}$) of 30940 $M^{-1}cm^{-1}$ for SPM-1, and 34950 $M^{-1}cm^{-1}$ for SPM-1/Sfh-I (calculated from aromatic residues using Expasy ProtParam, available at http://web.expasy.org/protparam/).

Biochemical Characterization of the Enzymes

The metal content in the protein samples was determined under denaturing conditions using the colorimetric metal chelator 4-(2-pyridylazo) resorcinol (PAR) as described previously (32). Circular Dichroism spectroscopy was used to test the global folding state of proteins. CD spectrums were performed at the far-UV (195-250 nm) on a Jasco J-810 spectropolarimeter with

quartz cuvettes of 0.1 and enzyme concentrations of 10 µM in 20 mM phosphate pH 7.5 at 25 °C. The metal content of SPM-1/SfhI was performed by reaction of 10 µM of the denatured protein with Ellman's reagent (33) in a buffer containing Hepes 10 mM, NaCl 200 mM, guanidine chloride 4 M, EDTA 50 mM, pH 7.4. Absorbance at 412 nm was measured and the value was extrapolated to a "free-thiols" calibration curve done with reduced glutathione (SIGMA).

Protein melting curves were obtained from samples aliquoted in 96-well plates using a RealPlex quantitative PCR instrument (Eppendorf), with SYPRO Orange dye (Sigma-Aldrich) as the fluorescent probe (34). A uniform final concentration of 30 X (supplied as a 5000 X stock solution) was used in all experiments. The dye was excited at 465 nm and emission recorded at 580 nm using the instrument's filters. A heating ramp of 1°C/min from 20°C to 95°C was used, and one data point acquired for each degree increment. The reactions were performed in 20 µl volume containing HEPES 10 mM pH 7.5, NaCl 200 mM with or without 10 µg of protein. Lysozyme (10 µg) was used as positive control. All experiments were done in triplicate, from two independent protein preparations. Values of Tm were obtained from non-linear fit of the melting curves to a sigmoid equation.

Steady State Kinetic Assays

Kinetic parameters were determined spectrophotometrically using a Jasco V-670 spectrophotometer following initial reaction rates at different substrate concentrations. To estimate the antibiotic hydrolysis the following differential molar extinction coefficients were used: cefuroxime, $\Delta\varepsilon_{260\ nm} = -7{,}600\ M^{-1}cm^{-1}$; cephaloridine, $\Delta\varepsilon_{260\ nm} = -13{,}600\ M^{-1}cm^{-1}$; cefotaxime, $\Delta\varepsilon_{260\ nm} = -7{,}500\ M^{-1}cm^{-1}$; ceftazidime $\Delta\varepsilon_{260\ nm} = -9{,}000\ M^{-1}cm^{-1}$; imipenem, $\Delta\varepsilon_{300nm} = -9{,}000\ M^{-1}cm^{-1}$; benzylpenicillin, $\Delta\varepsilon_{235\ nm} = -775\ M^{-1}cm^{-1}$ and piperacillin, $\Delta\varepsilon_{235\ nm} =$

−820 $M^{-1}cm^{-1}$. Reaction medium was 10 mM HEPES pH 7.5, 200 mM NaCl and 5 µM ZnSO4 at 30 °C. The plots of the dependence of initial rates on substrate concentration were fitted to the Michaelis-Menten equation using SigmaPlot 12.0. Reported kinetic parameters correspond to the average of at least two determinations with independent protein samples. The k_{cat} values were corrected by the Zn(II) content of the protein samples as previously described (35). Antibiotics were purchased from Sigma-Aldrich, with the exception of imipenem (USP Pharmacopeia). All of them had a purity >95%.

Molecular Dynamics Simulations

We performed 100 ns MD simulations using AMBER14 package (23) starting from the crystal structure of SPM-1 in the open and close moiety (PDB code 2FHX and 4BP0) (14, 24) and Sfh-I (PDB code 3SD9). As crystallization of SPM-1^{open} was achieved with a vacant Zn2 site, the metal site structure of SPM-1 was reconstructed by aligning it to the geometry of the Zn2 site of the homologous enzyme *B. cereus* BcII (PDB code 1BC2) (36, 37) as in our previous work (7). The initial structure of the chimeric protein SPM-1/Sfh-I was built *in-silico* through homology modelling by Modeller (Version 9.18) (38). To build our model we used both structures of SPM-1 and Sfh-I as templates. We used the same protocol to perform MD simulations as in our previous work (7, 39). Briefly, the systems were immersed in a box of water molecules TIP3P (40) and were simulated using periodic boundary conditions and Ewald sums for treating long-range electrostatic interactions (41). The SHAKE algorithm was applied to all hydrogen-containing bonds (42). Parm99 and TIP3P force fields implemented in AMBER were used to describe the protein and water, respectively (23). The force field of the active site (Zn, $^{-}$OH, Asp, Cys and His) was taken from the literature (43). The temperature and pressure were controlled by the Berendsen thermostat and barostat respectively, as implemented in

AMBER (23). Cut-off values used for the van der Waals interactions were 10 Å. Each initial system was minimized using a multistep protocol, then heated from 0 to 300 K, and finally a short simulation at constant temperature of 300 K, under constant pressure of 1 bar, was performed to allow the systems to reach proper density. These equilibrated structures were the starting point for 100 ns of MD simulations at 300 K in the NVT ensemble.

Brownian Dynamics Simulations

We calculated the collision probability between the different enzymes and the substrate using Brownian Dynamics simulations (44). The BD simulations were executed through the BrownDye package (45). The electrostatic potentials of the enzymes and substrates were calculated using the Adaptive Poisson Boltzman Solver (APBS) package (46). Substrate was started at an arbitrary distance (~20 Å) from the Zn2 center. 2,000,000 BD trajectories were performed starting from different enzyme configurations, which were taken from equilibrium MD simulations. Association probabilities were computed using the fraction of the trajectories that "reacted", according to the chosen reaction criterion. Reaction criterion used was the Zn2...N (β-lactam ring) distance, in which a value of 8 Å was considered the end of the BD trajectory. The relative probability of association was calculated by dividing the successful trajectories of each enzyme by the reactive trajectories of the enzyme SPM-1^{open}.

ACKNOWLEDGEMENTS

We thank Alejandro Viale (IBR) for providing GroEL antibodies. This research was supported by grants from the National Institutes of Health (R01AI100560) and Agencia Nacional de Promoción Científica y Tecnológica (ANPCyT) to AJV. LJG, DMM and AJV are staff members of CONICET. CSV and JCP are fellowships.

REFERENCES

1. Patel G, Bonomo RA. 2013. “Stormy waters ahead”: Global emergence of carbapenemases. Front Microbiol.
2. Crowder MW, Spencer J, Vila AJ. 2006. Metallo-beta-lactamases: Novel weaponry for antibiotic resistance in bacteria. Acc Chem Res 39:721–728.
3. Walsh TR, Toleman M a., Poirel L, Nordmann P. 2005. Metallo- -Lactamases: the Quiet before the Storm? Clin Microbiol Rev 18:306–325.
4. Nordmann P, Poirel L, Mark A. T, Timothy R. W. 2011. Does broad-spectrum β-lactam resistance due to NDM-1 herald the end of the antibiotic era for treatment of infections caused by Gram-negative bacteria? J Antimicrob Chemother 66:689–692.
5. Palzkill T. 2013. Metallo-B-lactamase structure and function. Ann N Y Acad Sci 1277:91–104.
6. Bebrone C. 2007. Metallo-β-lactamases (classification, activity, genetic organization, structure, zinc coordination) and their superfamily. Biochem Pharmacol 74:1686–1701.
7. González LJ, Moreno DM, Bonomo RA, Vila AJ. 2014. Host-Specific Enzyme-Substrate Interactions in SPM-1 Metallo-β-Lactamase Are Modulated by Second Sphere Residues. PLoS Pathog 10.
8. Widmann M, Pleiss J, Oelschlaeger P. 2012. Systematic analysis of metallo-β-lactamases using an automated database. Antimicrob Agents Chemother 56:3481–3491.
9. Materon IC, Beharry Z, Huang W, Perez C, Palzkill T. 2004. Analysis of the context dependent sequence requirements of active site residues in the metallo-beta-lactamase IMP-1. J Mol Biol 344:653–63.
10. Materon IC, Palzkill T. 2001. Identification of residues critical for metallo-beta-lactamase

function by codon randomization and selection. Protein Sci 10:2556–2565.

11. Sun Z, Mehta SC, Adamski CJ, Gibbs RA, Palzkill T. 2016. Deep Sequencing of Random Mutant Libraries Reveals the Active Site of the Narrow Specificity CphA Metallo-β-Lactamase is Fragile to Mutations. Sci Rep 6.

12. Rasia RM, Vila AJ. 2004. Structural determinants of substrate binding to Bacillus cereus metallo-beta-lactamase. J Biol Chem 279:26046–51.

13. Rasmussen BA, Bush K. 1997. Carbapenem-hydrolyzing beta-lactamases. Antimicrob Agents Chemother 41:223–32.

14. Murphy TA, Catto LE, Halford SE, Hadfield AT, Minor W, Walsh TR, Spencer J. 2006. Crystal structure of Pseudomonas aeruginosa SPM-1 provides insights into variable zinc affinity of metallo-β-lactamases. J Mol Biol 357:890–903.

15. Toleman M a, Simm AM, Murphy T a, Gales AC, Biedenbach DJ, Jones RN, Walsh TR. 2002. Molecular characterization of SPM-1, a novel metallo-beta-lactamase isolated in Latin America: report from the SENTRY antimicrobial surveillance programme. J Antimicrob Chemother 50:673–679.

16. Fonseca F, Bromley EHC, Saavedra MJ, Correia A, Spencer J. 2011. Crystal structure of serratia fonticola Sfh-I: Activation of the nucleophile in mono-zinc metallo-β-lactamases. J Mol Biol 411:951–959.

17. González LJ, Bahr G, Nakashige TG, Nolan EM, Bonomo RA, Vila AJ. 2016. Membrane anchoring stabilizes and favors secretion of New Delhi metallo-β-lactamase. Nat Chem Biol 12:516–22.

18. Garcia-Saez I, Docquier JD, Rossolini GM, Dideberg O. 2008. The Three-Dimensional Structure of VIM-2, a Zn-β-Lactamase from Pseudomonas aeruginosa in Its Reduced and Oxidised Form. J Mol Biol 375:604–611.

19. Hernandez Valladares M, Felici a, Weber G, Adolph HW, Zeppezauer M, Rossolini GM, Amicosante G, Frère JM, Galleni M. 1997. Zn(II) dependence of the Aeromonas hydrophila AE036 metallo-beta-lactamase activity and stability. Biochemistry 36:11534–11541.

20. Simona F, Magistrato A, Vera DMA, Garau G, Vila AJ, Carloni P. 2007. Protonation state and substrate binding to B2 metallo-β-lactamase CphA from Aeromonas hydrofila. Proteins Struct Funct Genet 69:595–605.

21. Simona F, Magistrato A, Dal Peraro M, Cavalli A, Vila AJ, Carloni P. 2009. Common mechanistic features among metallo-β-lactamases: A computational study of aeromonas hydrophila CphA enzyme. J Biol Chem 284:28164–28171.

22. Fonseca F, Arthur CJ, Bromley EHC, Samyn B, Moerman P, Saavedra MJ, Correia A, Spencer J. 2011. Biochemical characterization of Sfh-I, a subclass B2 metallo-β-lactamase from Serratia fonticola UTAD54. Antimicrob Agents Chemother 55:5392–5395.

23. Case DA, Babin V, Berryman JT, Betz RM, Cai Q, Cerutti DS, T.E. Cheatham III, Darden TA, Duke RE, Gohlke H, Goetz AW, Gusarov S, Homeyer N, Janowski P, Kaus J, Kolossváry I, Kovalenko A, Lee TS, LeGrand S, Luchko T, Luo R, Madej B, Merz KM, Paesani F, Roe KP. 2014. AMBER 14, University of California, San Francisco.

24. Brem J, Struwe WB, Rydzik AM, Tarhonskaya H, Pfeffer I, Flashman E, van Berkel SS, Spencer J, Claridge TDW, McDonough M a., Benesch JLP, Schofield CJ. 2015. Studying the active-site loop movement of the São Paolo metallo-β-lactamase-1. Chem Sci 6:956–963.

25. Abboud MI, Hinchliffe P, Brem J, Macsics R, Pfeffer I, Makena A, Umland KD, Rydzik AM, Li GB, Spencer J, Claridge TDW, Schofield CJ. 2017. 19F-NMR Reveals the Role

of Mobile Loops in Product and Inhibitor Binding by the S??o Paulo Metallo-??-Lactamase. Angew Chemie - Int Ed 56:3862–3866.

26. Huang Y, Huber G, Wang N, Minteer S, McCammon J. 2017. Brownian dynamic study of an enzyme metabolon in the TCA cycle: Substrate kinetics and channeling. Protein Sci.

27. Moali C, Anne C, Lamotte-Brasseur J, Groslambert S, Devreese B, Van Beeumen J, Galleni M, Frère JM. 2003. Analysis of the importance of the metallo-beta-lactamase active site loop in substrate binding and catalysis. Chem Biol 10:319–29.

28. Bottoni C, Perilli M, Marcoccia F, Piccirilli A, Pellegrini C, Colapietro M, Sabatini A, Celenza G, Kerff F, Amicosante G, Galleni M, Mercuri PS. 2016. Kinetic studies on CphA mutants reveal the role of the P158-P172 loop in activity versus carbapenems. Antimicrob Agents Chemother 60:3123–3126.

29. Choi KH, Kumar A, Schweizer HP. 2006. A 10-min method for preparation of highly electrocompetent Pseudomonas aeruginosa cells: Application for DNA fragment transfer between chromosomes and plasmid transformation. J Microbiol Methods 64:391–397.

30. Jensch T, Fricke B. 1997. Localization of alanyl aminopeptidase and leucyl aminopeptidase in cells of Pseudomonas aeruginosa by application of different methods for periplasm release. J Basic Microbiol 37:115–28.

31. Marchiaro P, Mussi MA, Ballerini V, Pasteran F, Viale AM, Vila AJ, Limansky AS. 2005. Sensitive EDTA-based microbiological assays for detection of metallo-β-lactamases in nonfermentative gram-negative bacteria. J Clin Microbiol 43:5648–5652.

32. Abriata LA, González LJ, Llarrull LI, Tomatis PE, Myers WK, Costello AL, Tierney DL, Vila AJ. 2008. Engineered mononuclear variants in Bacillus cereus metallo-β-lactamase BcII are inactive. Biochemistry 47:8590–8599.

33. Ellman GL. 1959. Tissue sulfhydryl groups. Arch Biochem Biophys 82:70–77.

34. Lo MC, Aulabaugh A, Jin G, Cowling R, Bard J, Malamas M, Ellestad G. 2004. Evaluation of fluorescence-based thermal shift assays for hit identification in drug discovery. Anal Biochem 332:153–159.

35. Llarrull LI, Tioni MF, Kowalski J, Bennett B, Vila AJ. 2007. Evidence for a dinuclear active site in the metallo-beta-lactamase BcII with substoichiometric Co(II). A new model for metal uptake. J Biol Chem 282:30586–95.

36. Fabiane SM, Sohi MK, Wan T, Payne DJ, Bateson JH, Mitchell T, Sutton BJ. 1998. Crystal structure of the zinc-dependent β-lactamase from Bacillus cereus at 1.9 Å resolution: Binuclear active site with features of a mononuclear enzyme. Biochemistry 37:12404–12411.

37. Carfi a, Pares S, Duée E, Galleni M, Duez C, Frère JM, Dideberg O. 1995. The 3-D structure of a zinc metallo-beta-lactamase from Bacillus cereus reveals a new type of protein fold. EMBO J 14:4914–4921.

38. Webb B, Sali A. 2014. Comparative protein structure modeling using MODELLER. Curr Protoc Bioinforma 2014:5.6.1-5.6.32.

39. Morán-Barrio J, Lisa MN, Larrieux N, Drusin SI, Viale AM, Moreno DM, Buschiazzo A, Vila AJ. 2016. Crystal structure of the metallo-β-lactamase GOB in the periplasmic dizinc form reveals an unusual metal site. Antimicrob Agents Chemother 60:6013–6022.

40. Jorgensen WL, Chandrasekhar J, Madura JD, Impey RW, Klein ML. 1983. Comparison of simple potential functions for simulating liquid water. J Chem Phys 79:926–935.

41. Luty BA, Tironi IG, van Gunsteren WF. 1995. Lattice-sum methods for calculating electrostatic interactions in molecular simulations. J Chem Phys 103:3014–3021.

42. Ryckaert JP, Ciccotti G, Berendsen HJC. 1977. Numerical-Integration of Cartesian Equations of Motion of a System with Constraints - Molecular-Dynamics of N-Alkanes. J

Comput Phys 23:327–341.

43. Suárez D, Brothers EN, Merz KM. 2002. Insights into the structure and dynamics of the dinuclear zinc β-lactamase site from Bacteroides fragilis. Biochemistry 41:6615–6630.

44. Northrup SH, Allison SA, McCammon JA. 1984. Brownian dynamics simulation of diffusion-influenced bimolecular reactions. J Chem Phys 80:1517–1524.

45. Huber GA, McCammon JA. 2010. Browndye: A software package for Brownian dynamics. Comput Phys Commun 181:1896–1905.

46. Baker NA, Sept D, Joseph S, Holst MJ, McCammon JA. 2001. Electrostatics of nanosystems: Application to microtubules and the ribosome. Proc Natl Acad Sci 98:10037–10041.

FIGURE LEGENDS

Figure 1. Design of SPM-1/Sfh-I. (A) Structural alignment of SPM-1 (black/red) and Sfh-I (grey/yellow) showing substitutions (1:L119T; 2:Y223N; 3:D226F) and swapping of sequence insertions to render SPM-1/Sfh-I. (B) Sequence swapping displayed on crystal structures of SPM-1 (PDB: 2FHX) and Sfh-I (PDB: 3SD9). (C) Representation of native interactions accomodating α3 insertion in Sfh-I. Zinc ions are depicted as purple spheres.

Figure 2. Western-blot of spheroplasts and periplasmic fractions from *P. aeruginosa* PAO1 and *E. coli* DH5α, producers of SPM-1 or SPM-1/Sfh-I. Cells containing the empty vector (-) were used as control. Anti-Strep-tag antibody was used to assess SPM-1 or SPM-1/Sfh-I production, while GroEL and MBP are spheroplasts and periplasm markers respectively.

562 **Figure 3.** Folding and thermal stability of SPM-1 and SPM-1/Sfh-1. (A) Far UV CD spectrum of
563 wild-type SPM-1 (solid line) and SPM-1/Sfh-I hybrid protein (broken line). (B) Thermal
564 denaturation of SPM-1 (solid line) and SPM-1/Sfh-I (broken line) followed by thermal shift (Tm
565 SPM-1/Sfh-I= 51 ± 1 °C, Tm SPM-1= 75 ± 0.5 °C).
566
567 **Figure 4.** (A) Representative snapshots of the MD simulations of SPM-1^{open} (red), SPM-1/Sfh-
568 I^{open} (violet), SPM-1/Sfh-I^{closed} (cyan), SPM-1^{closed} (pink) and Sfh-I (dark yellow), showing the
569 accessibility of the active site. (B) Relative probability of association of the enzymes with PenG.
570
571 **TABLES**
572 **Table 1.** MIC values for wild type SPM-1 and SPM-1/Sfh-I expressing bacterial strains. Both *E.*
573 *coli* and *P. aeruginosa* were transformed with expression vectors for SPM-1 and SPM-1/Sfh-I
574 enzymes and challenged to different β-lactam antibiotics. Cells containing the empty vector (-)
575 were used as control. MICs were measured in triplicate.
576

	MIC (μg/ml)					
	E. coli DH5α			*P. aeruginosa* PAO1		
	SPM-1	SPM-1/Sfh-I	(–)	SPM-1	SPM-1/Sfh-I	(–)
Ceftazidime	128	0.125	0.25	512	0.5	0.5
Cefotaxime	32	0.06	0.06	ND	ND	ND
Piperacillin	8 - 16	2	2	64 - 128	2	2
Imipenem	1	0.03	0.06	64	1	1

577
578
579

580 **Table 2.** β-Lactam hydrolysis parameters of SPM-1 and SPM-1/Sfh-1. β-Lactamase activities
581 were measured at 30 °C in Hepes 10 mM, NaCl 200 mM, pH 7.5 supplemented with 5 µM
582 Zn(II). Data come from three independent experiments, and are presented as mean ± s.d.

583

	SPM-1			SPM-1/Sfh-I		
	k_{cat} (s^{-1})	K_M (µM)	k_{cat}/K_M ($\mu M^{-1}s^{-1}$)	k_{cat} (s^{-1})	K_M (µM)	k_{cat}/K_M ($\mu M^{-1}s^{-1}$)
Cefotaxime	57 ± 15	39 ± 12	1.5 ± 0.8	720 ± 260	183 ± 80	3.9 ± 1.0
Ceftazidime	270 ± 36	1020 ± 84	0.26 ± 0.06	ND[b]	ND[b]	0.37 ± 0.12[a]
Cefuroxime	86 ± 19	14 ± 5	6.3 ± 3.6	ND[b]	ND[b]	2.0 ± 1.0[a]
Cefaloridine	300 ± 45	58 ± 10	5.2 ± 1.7	ND[b]	ND[b]	1.1 ± 0.4[a]
PenG	140 ± 20	59 ± 15	2.3 ± 1.0	29 ± 1	609 ± 98	0.048 ± 0.026
Piperacillin	240 ± 30	120 ± 30	2.0 ± 0.8	71 ± 22	1200 ± 200	0.059 ± 0.028
Imipenem	68 ± 19	100 ± 40	0.67 ± 0.42	4 ± 1	107 ± 17	0.040 ± 0.016

584 [a]Determined at low concentrations of substrate

A

```
                                                                                1
SPM-1           SDHVDLPYNLTATKIDSDVFVVTDRDFYSSNVLVAKMLDGTVVIVSSPFENLGTQTLMDWVAKTMKPKKVVAINTHFHLD
Sfh-I           ----MSEKNLTLTHFKGPLYIVEDKEYVQENSMVYIGTDG-ITIIGATWTPETAETLYKEIRKVSPLPINEVINTNYHTD
SPM-1/Sfh-I     SDHVDLPYNLTATKIDSDVFVVTDRDFYSSNVLVAKMLDGTVVIVSSPFENLGTQTLMDWVAKTMKPKKVVAINTHFHTD
                                          Sequence replacement
SPM-1           GTGGNEIYKKMGAETWSSDLTKQLRLEENKKDRIKAAEFYKNEDLKRRI----LSSHPVPADNVFDLKQGKVFSFSNELV
Sfh-I           RAGGNAYWKTLGAKIVATQMTYDLQKSQW----------GSIVNFTRQGNNKYPNLEKSLPDTVFPG--DFNLQ--NGSI
SPM-1/Sfh-I     GTGGNEIYKKMGAETWSSDLTKQLRLEQW----------GSIVNFTRQGNNKYPNLEKSLPDNVFDLKQGKVFSFSNELV
                                                  2  3
SPM-1           EVSFPGPAHSPDNVVVYFPKKKLLFGGCMIKPKELGYLGDANVKAWPDSARRLKKF------DAKIVIPGHGEW-GGPEM
Sfh-I           RAMYLGEAHTKDGIFVYFPAERVLYGNCILKE-NLGNMSFANRTEYPKTLEKLKGLIEQGELKVDSIIAGHDTPIHDVGL
SPM-1/Sfh-I     EVSFPGPAHSPDNVVVYFPKKKLLFGGCMIKPKELGNLGFANVKAWPDSARRLKKF------DAKIVIPGHGEW-GGPEM

SPM-1           VNKTIKVAEKAVGEMRL
Sfh-I           IDHYLTLLEKAPK----
SPM-1/Sfh-I     VNKTIKVAEKAVGEMRL
```

B

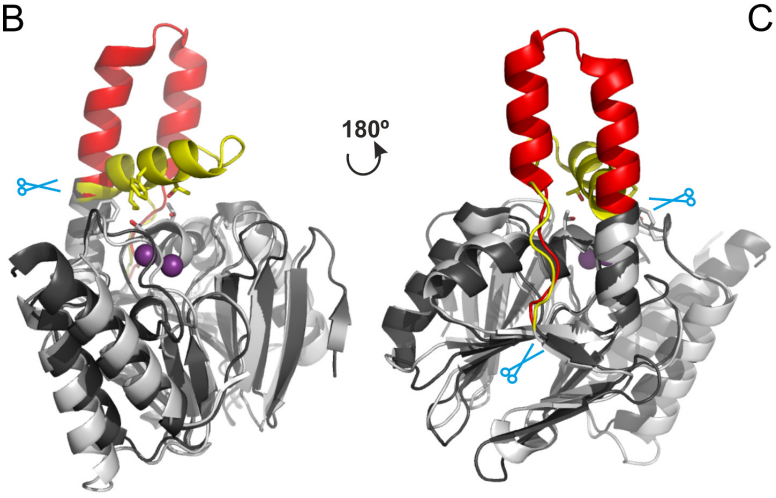

C